ADVANCED FUNCTIONAL MATERIALS
www.afm-journal.de

Engineered Vascularized Flaps, Composed of Polymeric Soft Tissue and Live Bone, Repair Complex Tibial Defects

*Idan Redenski, Shaowei Guo, Majd Machour, Ariel Szklanny, Shira Landau, Ben Kaplan, Roberta I. Lock, Yankel Gabet, Dana Egozi, Gordana Vunjak-Novakovic, and Shulamit Levenberg**

Functional regeneration of complex large-scaled defects requires both soft- and hard-tissue grafts. Moreover, bone constructs within these grafts require an extensive vascular supply for survival and metabolism during the engraftment. Soft-tissue pedicles are often used to vascularize bony constructs. However, extensive autologous tissue-harvest required for the fabrication of these grafts remains a major procedural drawback. In the current work, a composite flap is fabricated using synthetic soft-tissue matrices and decellularized bone, combined in vivo to form de novo composite tissue with its own vascular supply. Pre-vascularization of the soft-tissue matrix using dental pulp stem cells (DPSCs) and human adipose microvascular endothelial cells (HAMECs) enhances vascular development within decellularized bones. In addition, osteogenic induction of bone constructs engineered using adipose derived mesenchymal stromal cells positively affects micro-capillary organization within the mineralized component of the neo-tissue. Eventually, these neo-tissues used as axial reconstructive flaps support long-term bone defect repair, as well as muscle defect bridging. The composite flaps described here may help eliminate invasive autologous tissue-harvest for patients in need of viable grafts for transplantation.

1. Introduction

Tissue loss due to trauma, infection or pathological lesions can result in large osteo-muscular defects. Despite the regenerative potential of soft and hard tissues, healing of substantial defects with compromised vascular support requires large, vascularized tissue flaps. While harvested autografts currently serve as the clinical gold standard for major reconstructions, they are still associated with major disadvantages, such as limited autograft volume, tissue site morbidity and substantial post-operative complications.[1,2] As a result, harnessing the innate regenerative potential to repair tissue defects, by the use of extracellular matrix (ECM)-based biomaterials and tissue constructs has gained much attention.[3–7] ECM-based scaffolds have proven effective in supporting tissue regeneration, by eliciting a preferred cellular response and biological recognition with only minor inflammatory responses.[8–10] Decellularized bone (DCB), a clinically approved ECM-based material, has been shown to support bone regeneration by enabling osteogenic induction, tissue ingrowth, and fabrication of complex anatomically correct bone grafts.[11,12]

Survival of engineered grafts at a surgical site critically depends on host capillary invasion and vascular network development within the tissue constructs.[13–15] The lack of initial vascularization after implantation and rapid host-to-graft vascular connectivity are the main causes of bioengineered constructs

Dr. I. Redenski, Dr. S. Guo, M. Machour, A. Szklanny, Dr. S. Landau, B. Kaplan, Prof. S. Levenberg
Department of Biomedical Engineering
Technion—Israel Institute of Technology
Haifa 32000, Israel
E-mail: Shulamit@bm.technion.ac.il

Dr. S. Guo
The First Affiliated Hospital
Shantou University Medical College
Shantou 515000, China

The ORCID identification number(s) for the author(s) of this article can be found under https://doi.org/10.1002/adfm.202008687.

DOI: 10.1002/adfm.202008687

R. I. Lock, Prof. G. Vunjak-Novakovic
Department of Biomedical Engineering
Columbia University
New York, NY 10032, USA

Prof. Y. Gabet
Department of Anatomy and Anthropology
Sackler Faculty of Medicine
Tel-Aviv University
Tel-Aviv 6997801, Israel

Dr. D. Egozi
Department of Plastic and Reconstructive Surgery
Kaplan Hospital
Rehovot and the Hebrew University
Jerusalem 7661041, Israel

failure.[16–18] Bone grafts require rapid anastomosis with the host vasculature for nutrient supply,[19] because of high metabolic activity of bone cells, and diffusional penetration depths of oxygen that are as low as 200 μm.[20]

Creation of tissue engineered bone grafts (TEBGs) with a mature capillary plexus remains a major challenge in the field. Several strategies have been proposed to accelerate the establishment of a vascular network within implanted bone constructs such as growth factor incorporation and micro-architectural design of capillaries.[21,22] Another approach implements vascular and micro-surgical techniques to facilitate capillary ingrowth from surrounding tissues.[23–26] While these procedures involving macro-vessel manipulation may aid to the initial vascular penetration into grafts, these methodologies are technically challenging[21] and rarely used to support bone defect repair.[26,27] A promising approach is the utilization of endothelial cells (ECs) and supporting cells to induce pre-vascularization of tissue constructs.[28–30] DPSCs, a versatile cell population residing in the dental pulp have been shown to support endothelial organization,[31] and adipose-derived MSCs have been shown to promote decellularized bones maturation and integration.[12] We hypothesize that engineered composite-tissue flaps based on pre-vascularized polymeric matrices, containing a vascularized decellularized bone seeded with MSCs, will facilitate bone defect repair and angiogenesis.

Our goal was to fabricate a de novo composite-tissue flap, comprised of vascularized soft and hard tissue components designed to bridge complicated tissue defects. The proposed approach involves pre-vascularization of tissue constructs using a co-culture of ECs and supporting cells. Decellularized bone matrix (DCBs) was then implanted in vivo within the vascularized bio-engineered scaffolds and wrapped around a major arteriovenous (AV) bundle, yielding a vascularized tissue composed of both soft and hard bioengineered constructs. We tested the capacity of these engineered composite tissues to heal tibial bone defect in rats, to demonstrate their regenerative potential.

2. Results

The composite-tissue fabrication process was based on several steps, leading to a vascularized bone with an active vascular network, embedded in a vascularized neo-tissue pedicle. First, to pre-vascularize soft tissue-matrices co-cultures of DPSCs and HAMECs were loaded onto synthetic scaffolds and ECs monocultures were used as controls (**Figure 1**-i). ZsGreen lentiviral-transduced HAMECs were used to enable identification of vascular development and capillary interaction during the engraftment process. Next, the pre-vascularized engineered

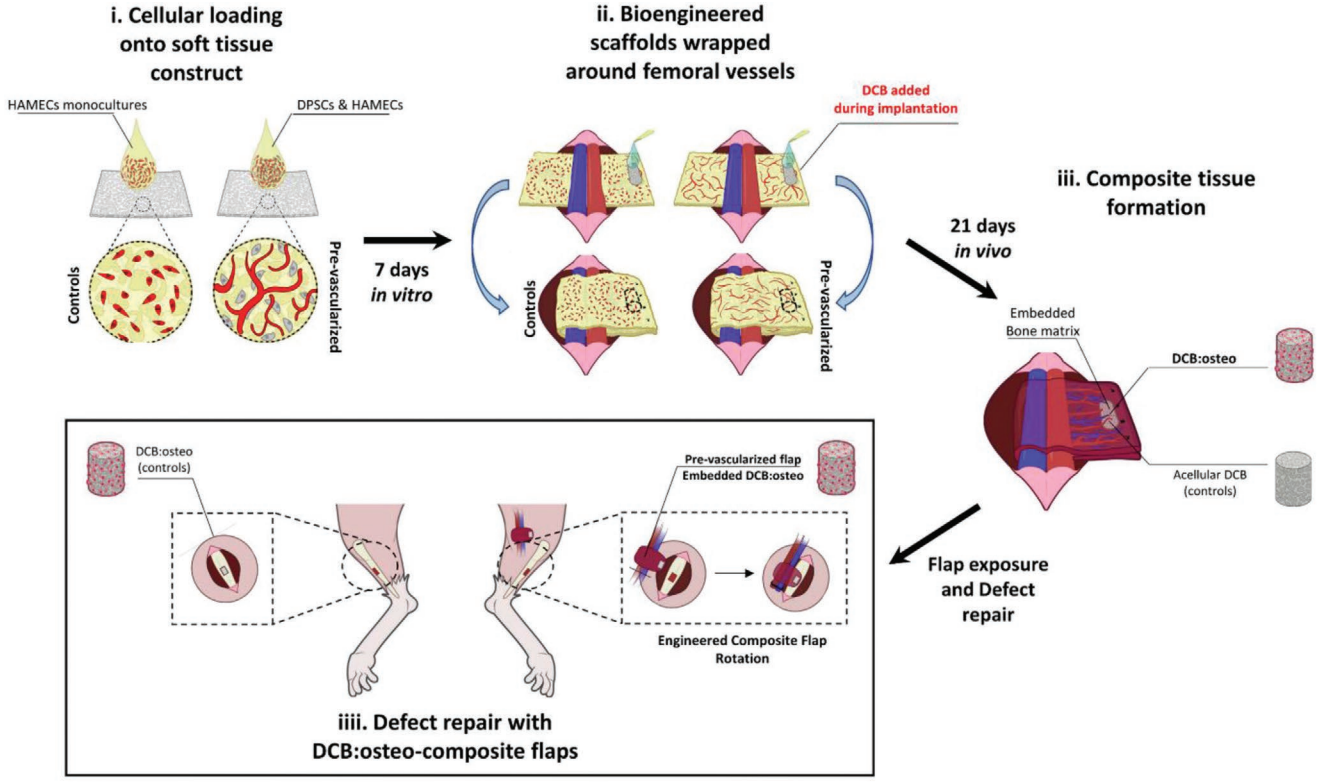

Figure 1. Schematics of experimental design. i) PLLA\PLGA scaffolds are seeded with either HAMECs monocultures or DPSC:HAMEC co-cultures for pre-vascularization of constructs. ii) Bioengineered scaffolds are wrapped around the femoral arteriovenous bundle, followed by attachment of a decellularized bone scaffold and construct closure. iii) 21 days after implantation composite tissues are exposed. Pre-vascularized tissues are fabricated and evaluated with either acellular or osteo-induced DCBs. iiii) A bone defect repair model is used to assess composite flap ability to support tissue repair.

scaffolds were assessed for their composite-tissue remodeling ability by utilizing the femoral AV implantation model, where a DCB was embedded during implantation of bioengineered constructs (Figure 1-ii,iii). Acellular and osteogenically induced bones were assessed for their integration and vascularization in vivo. Finally, to test the feasibility of the proposed methodology, composite tissues were mobilized as rotational flaps to support bone defect repair (Figure 1-iiii).

2.1. Pre-Vascularization of the Engineered Soft Tissue In Vitro

To fabricate highly vascularized bioengineered soft tissues that can support the vascularization of the DCB in vivo, ECs (HAMECs) were co-cultured with the supporting cells (DPSCs) (Figure 1) on PLLA/PLGA constructs, for 3 and 7 days. After both durations of incubation, cellular constructs exhibited vascular development, while HAMEC monoculture constructs showed no substantial vessel development (**Figure 2**A,B; Figure S1A,B, Supporting Information). Staining for ECM components further confirmed extensive vascular development in these pre-vascularized constructs, with collagen IV and elastin deposition evident around vessel networks in co-cultures, as opposed to unorganized and scarce fiber labeling in monoculture samples (Figure 2A). As for angiogenic factors secretion by seeded constructs after 3 and 7 days of culture, vascular endofthelial growth factor (VEGF) levels were significantly higher in pre-vascularized scaffolds, (Figure 2C). Angiopoietin1 (Ang1) was also highly elevated in pre-vascularized constructs as early as on day 3. In contrast, Angiopoietin2 (Ang2) levels were higher in monoculture controls as compared to co-cultures (Figure S1C,D, Supporting Information).

2.2. Formation of Vascularized Composite Tissue Flaps

To fabricate the vascularized composite-tissue flap and assess the impact of in vitro vascular organization on tissue development, bioengineered constructs were applied in a femoral AV bundle model. Control constructs (HAMEC monocultures without pre-vascularization) or pre-vascularized engineered soft-tissue constructs were implanted with a DCB, attached during implantation, using a biological fibrin solution (Figure 2D), to engineer the composite tissue. 3 weeks post-implantation, composite tissues were exposed and evaluated for perfusion and host vessel penetration. In vivo perfusion readings showed a nearly 50% increase in perfusion units per tissue area of pre-vascularized implants (Figure 2D,E) as compared to EC monoculture implants. High-resolution micro computed tumography (micro CT) scans of perfused explants indicated that DCBs within explanted tissues in the pre-vascularized group had been significantly penetrated by host vessels, as evident from the over threefold increase in vessel volume (Figure 2F,G) compared to the monoculture controls. Co-labeling of both graft ECM components as well as host vessels verified that laminin, elastin, and collagen IV secreted by bioengineered grafts, lined host micro-capillaries that had penetrated the engineered soft tissue (Figure 2H). Furthermore, human CD31, an established endothelial marker, was detected in samples from the pre-vascularized group, alongside host micro-vasculature (Figure S2, Supporting Information) during tissue remodeling.

2.3. Osteogenically Induced DCBs with Extensive Vascular Penetration In Vivo

To test the effect of vascularization within acellular versus osteoblast-seeded bone, human adipose-derived mesenchymal stromal cells were loaded onto DCBs and induced toward osteoblast differentiation. These DCB:osteo constructs showed cellular differentiation and osteogenic ECM secretion, as determined by Runt-related transcription factor 2 (Runx2), collagenI, and bonesialoprotein2 (BSP2) staining within DCB pore spaces (**Figure 3**A) as well as mineral deposition prior to implantation (Figure S3, Supporting Information). DCB:osteo or control acellular DCBs were co-implanted with the soft tissue around the AV bundle. DCB:osteo induced host vessel penetration into the bone scaffolds, as shown by laminin and alpha-smooth muscle actin (α-SMA) labeling, indicating vascular basement membrane fiber and pericyte organization. Laminin was closely distributed around infiltrating vessels as demonstrated by co-staining with host $CD31^+$ cells, and Runx2-positive cells were identified adjacent to penetrating capillaries within DCB:osteo scaffolds (Figure S4, Supporting Information). In acellular constructs, less co-localization of laminin with endothelial cells was evident, with a high incidence of laminin deposition unrelated to host vessels (Figure 3B,C). α-SMA staining showed pericyte organization around the vasculature, which was significantly higher in the DCB:osteo implants (6.1% ± 0.85% versus 2.6% ± 0.58%) compared to the acellular DCBs (Figure 3D,E). MicroCT angiography of perfused composite tissues indicated that DCB:osteo underwent higher vascular penetration, with a nearly fivefold increase in vessel volume (**Figure 4**A), higher inner-connectivity between penetrating vessels, as evident from Euler connectivity values (Figure 4C), and significantly larger proportion of large-diameter vessels (Figure 4D) compared to acellular DCB implants. Histological sections verified that DCB:osteo constructs were actively perfused, with erythrocyte-filled capillaries penetrating deep into bone pore spaces (Figure 4E).

2.4. Biological Bone Matrix in Composite Neo-Tissues Improved Anti-Inflammatory Host Response Compared to Synthetic Scaffolds

After demonstrating a favorable host response to biological bone matrix within pre-vascularized constructs, the remodeling potential of a synthetic biomaterial and tissue response were assessed. Mineralized polycaprolactone-hydroxyapetite (PCL-HA) scaffolds were seeded with MSCs which underwent osteogenic differentiation, (termed PCL-HA:osteo), as verified by Runx2, BSP2 and collagenI staining (Figure S5A, Supporting Information). On 21 days post-implantation, laser speckle contrast imaging (LSCI) readings indicated low perfusion in tissues enveloping the PCL-HA:osteo scaffolds compared to tissues containing DCB:osteo constructs (5.09% ± 1.2% versus 44.7% ± 7.3%, Figure S6A,B, Supporting Information). Gross

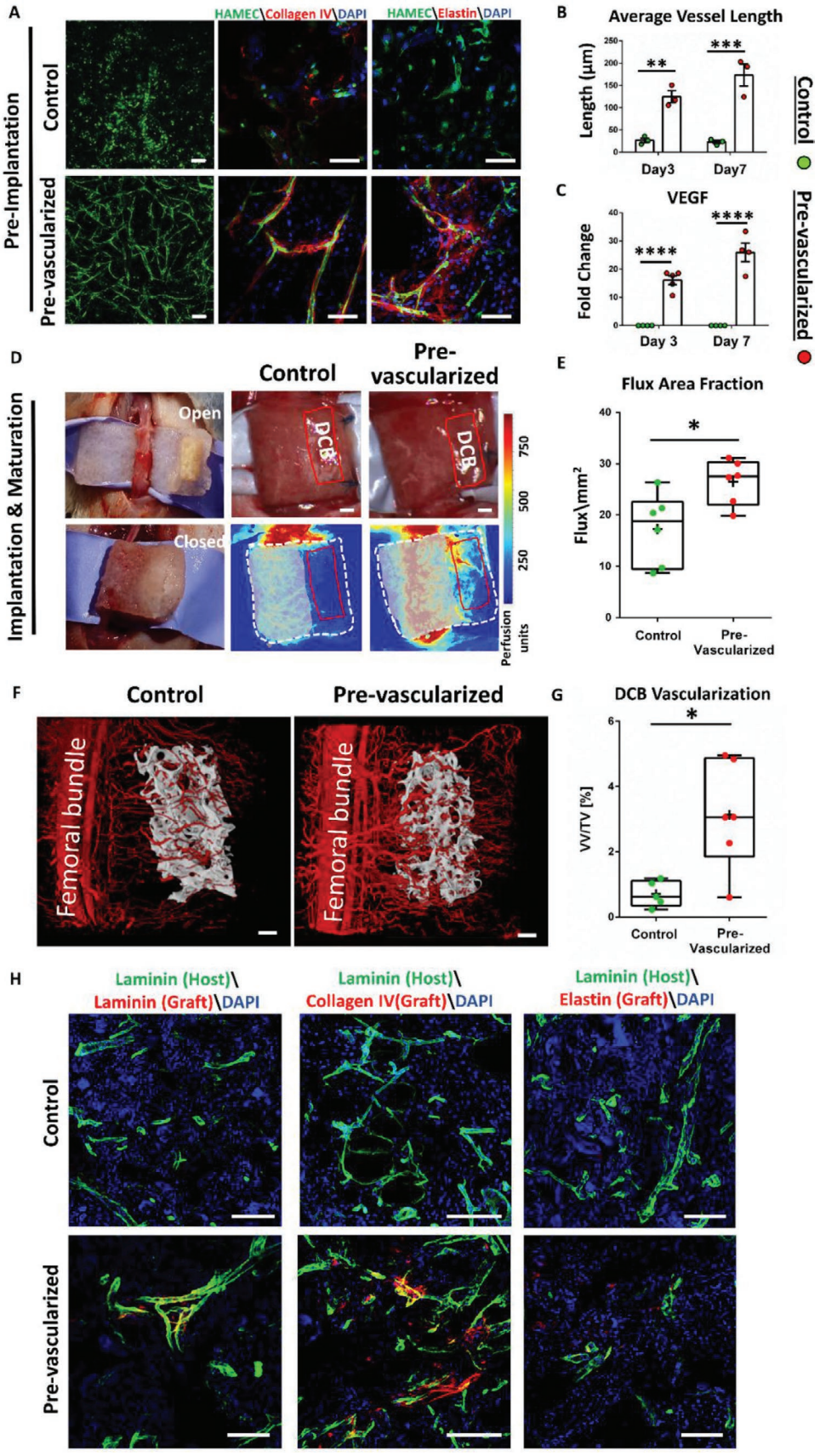

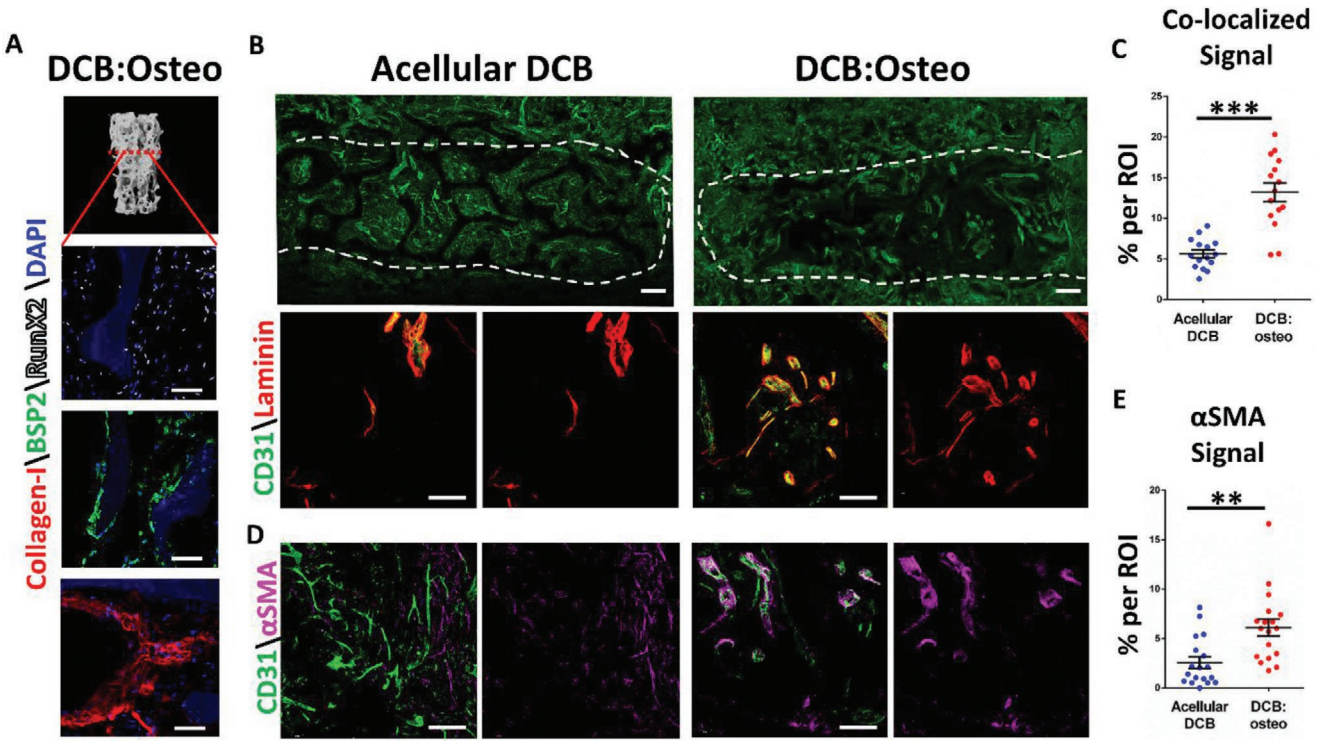

Figure 3. Osteogenically induced DCBs undergo extensive vascular penetration within forming tissues in vivo. A) Immunofluorescence used to verify in-vitro osteogenic induction and ECM secretion within DCB: osteo scaffolds, by staining for collagenI, BSP2 and Runx2. Scale bar = 100 µm. B,D) Confocal images of DCB and DCB:osteo scaffolds within composite tissues after 21 days in vivo, stained for CD31, laminin, and alpha smooth muscle actin; upper row depicts whole-tissue section tile-scans. White dashed lines outline bone scaffolds within composite tissues. Scale bars = 500, 50 µm C,E) Immunofluorescence co-labeling quantification of CD31 and laminin (C) and alpha smooth muscle actin signal (E). $n = 4$ animals per group for tissue sections analysis. Results are presented as mean ± s.e.m (*t*-test). Significance levels: $^{**}p < 0.01$, $^{***}p < 0.001$.

inspection revealed partial tissue dehiscence or construct deterioration on the surface of composite tissues enveloping the PCL-HA bony scaffolds, implying lower integration (Figure S6C, Supporting Information). Histological evaluation of the PCL-HA:osteo samples revealed a reactive cellular layer accumulating on the surface of the bone scaffold (**Figure 5**A). Within the scaffold pores, cellular density was substantially lower, with foreign body giant cells accumulating on the inner walls of the PCL-HA construct (Figure 5A,B). Continuous collagen fiber deposition across the engineered soft tissue and DCB:osteo interface was evident, with a higher cellular content within scaffold pores, in contrast to the PCL-HA:osteo group (Figure 5B–D).

To assess integration of the co-implanted biomaterials in vivo, the nature of the host response was examined at the engineered-tissue:bone-scaffold interface. The implanted PCL-HA:osteo tissues contained penetrating macrophages, 20.5% ± 4.4% of which were of M1 pro-inflammatory phenotype (labeled for CCR7 and CD68), while fewer than 5% of the cells in the DCB:osteo constructs expressed pro-inflammatory markers (Figure 5E,F). An opposite trend was registered for remodeling M2 macrophages, which comprised almost 20% of CD206-positive immune cells embedded in the DCB:osteo samples, and fewer than 8% of these cells embedded in PCL-HA:osteo scaffolds (Figure 5G,H). Immuno-histological examination of engineered tissues containing DCB:osteos indicated that cells committed to the osteogenic lineage were evident 3 weeks post-implantation, in contrast to the PCL-HA:osteo samples which showed only faint Runx2 signal (Figure 5I)

Figure 2. Pre-vascularization assessment of implanted soft tissue component within composite tissues. A) Confocal images of 7-day-incubated PLLA/PLGA scaffolds seeded with ECs monoculture (controls) and prevascularized scaffolds seeded with co-cultures of DPSCs and HAMECs. Left column: HAMEC-ZsGreen organization within scaffolds; middle and right columns: ECM components, that is, collagen IV (middle) and elastin (right) with HAMEC ECs (green) and DAPI (blue). Scale bar = 100 µm. B) Average vessel length determined at 3 days and 7 days post-seeding of controls (green) and pre-vascularized (red) scaffolds. C) VEGF secretion from controls (green) and pre-vascularized (red) scaffolds after 3 and 7 days of in vitro incubation. D) Left column: color images depicting co-implantation of DCBs and bioengineered PLLA/PLGA constructs; middle and right columns: color (upper row) and LSCI (lower row) images of engineered composite tissues after 21 days of in vivo incubation. Scale bar = 1 mm. E) Flux area fraction analysis of composite-tissue area. F,G) MicroCT scans of microfil-perfused explants: 3D visualization (F) and volumetric analysis (G) of vessels penetrating DCBs (VV/TV) within composite tissues. H) Confocal images of tissue sections from 21-day explants, labeled for host vessels (green) and graft ECM components: laminin (left column), collagen IV (middle column), and elastin (right column). Scale bar = 100 µm. Data represent $n = 6$ animals for flux study, $n = 5$–6 animals per group for microCT vascular exploration. Results are presented as mean ± s.e.m (*t*-test). Significance levels: $^{*}p < 0.05$, $^{**}p < 0.01$, $^{***}p < 0.001$, $^{****}p < 0.0001$.

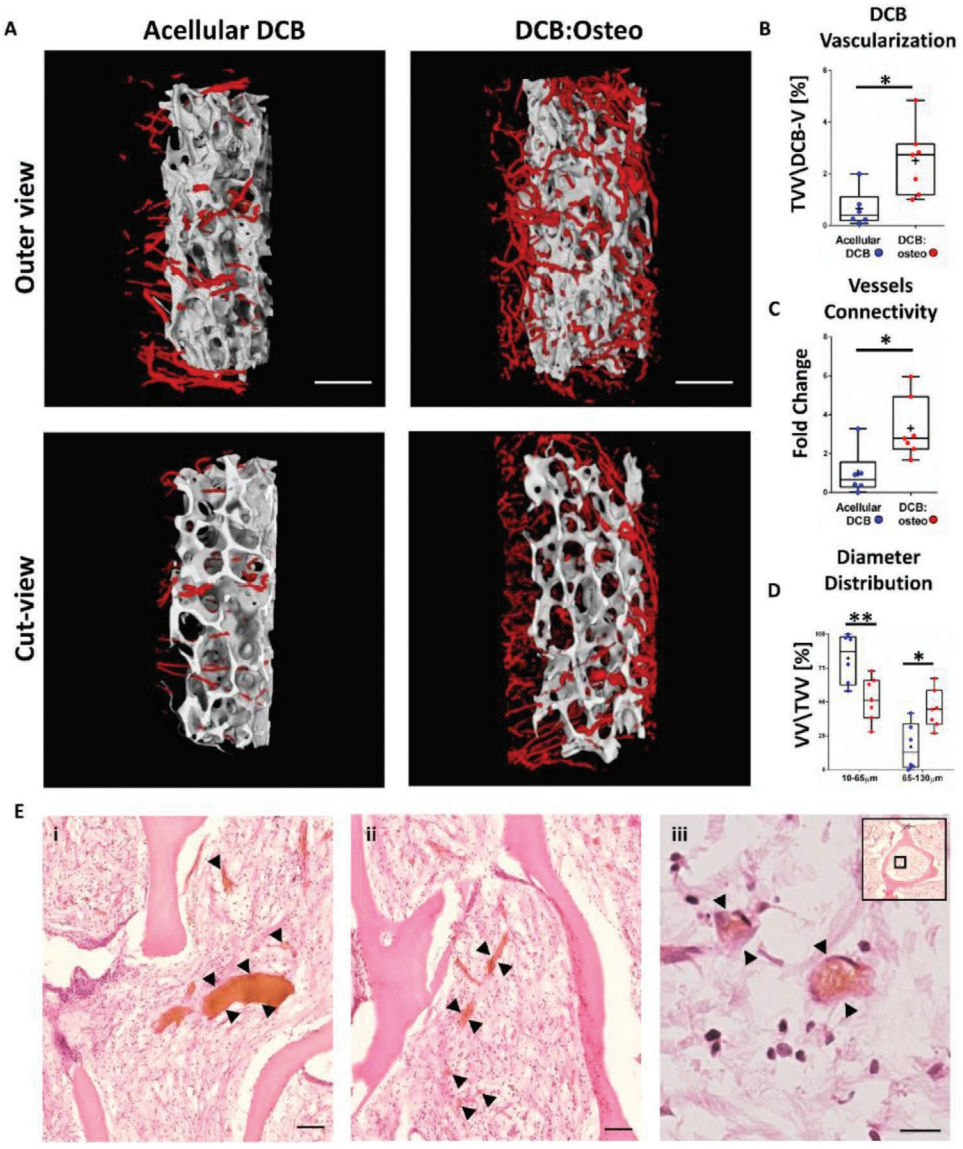

Figure 4. Volumetric and functional evaluation of formed capillaries within decellularized bone. A) MicroCT based 3D reconstruction of contrast-agent perfused DCBs within composite tissues. Images represent outer and inner views of the DCBs. Scale bar = 1 mm B–D) volumetric quantification and analysis of DCB-penetrating vessels (B), Euler connectivity (C), and diameter distribution (D) of DCB vascular networks. E) Representative H&E images of DCB pores within composite tissues 21 days after implantation. Black arrowheads mark functional capillaries and microcapillaries containing erythrocytes. Scale bar = 100 µm (i,ii), 20 µm (iii). n = 6–7 animals for microCT vascular analysis. Results are presented as mean ± s.e.m (t-test). Significance levels: $*p < 0.05$, $**p < 0.01$.

2.5. Engineered Composite Tissues Utilized as Surgical Flaps Support Bone Defect Repair

To gain an understanding on the potential of composite-tissue flaps to support a bone defect repair process, 21-day-old composite flaps containing a DCB:osteo were applied to repair a monocortical tibial defect (Figure 1-iiii; Figure S8A, Supporting Information). Rectangular 2 ×2 × 5 mm defects were created and repaired either by rotating the composite tissue with the bone scaffold attachment or by direct press-fitting of naïve non-vascularized DCB:osteo scaffolds as a control (Figure 1-iiii). In vivo microCT scans of defects 2 weeks after surgeries demonstrated similar BV/TV values, indicating that mineralized tissues were primarily comprised of pre-existing bone and implanted scaffolds (**Figure 6**B). Defect filling rates were similar between groups at this stage (Figure S8B, Supporting Information). Notable differences in total deposited mineralized tissue emerged 5 weeks after implantation, reaching over 73% in the composite flap and 63% in the DCB:osteo-only groups (Figure 6A,B). A significant reduction as of week 5 from implantation in the percentage of low calcified bone (LCB) within the defects treated with composite flaps was noted, starting with less than 20% LCB and reaching less than 10% by week 8 (Figure 6C). In the control group, the relative proportion of LCB dropped to 15% by week 8. As for the proportion of highly calcified bone (HCB), a constant

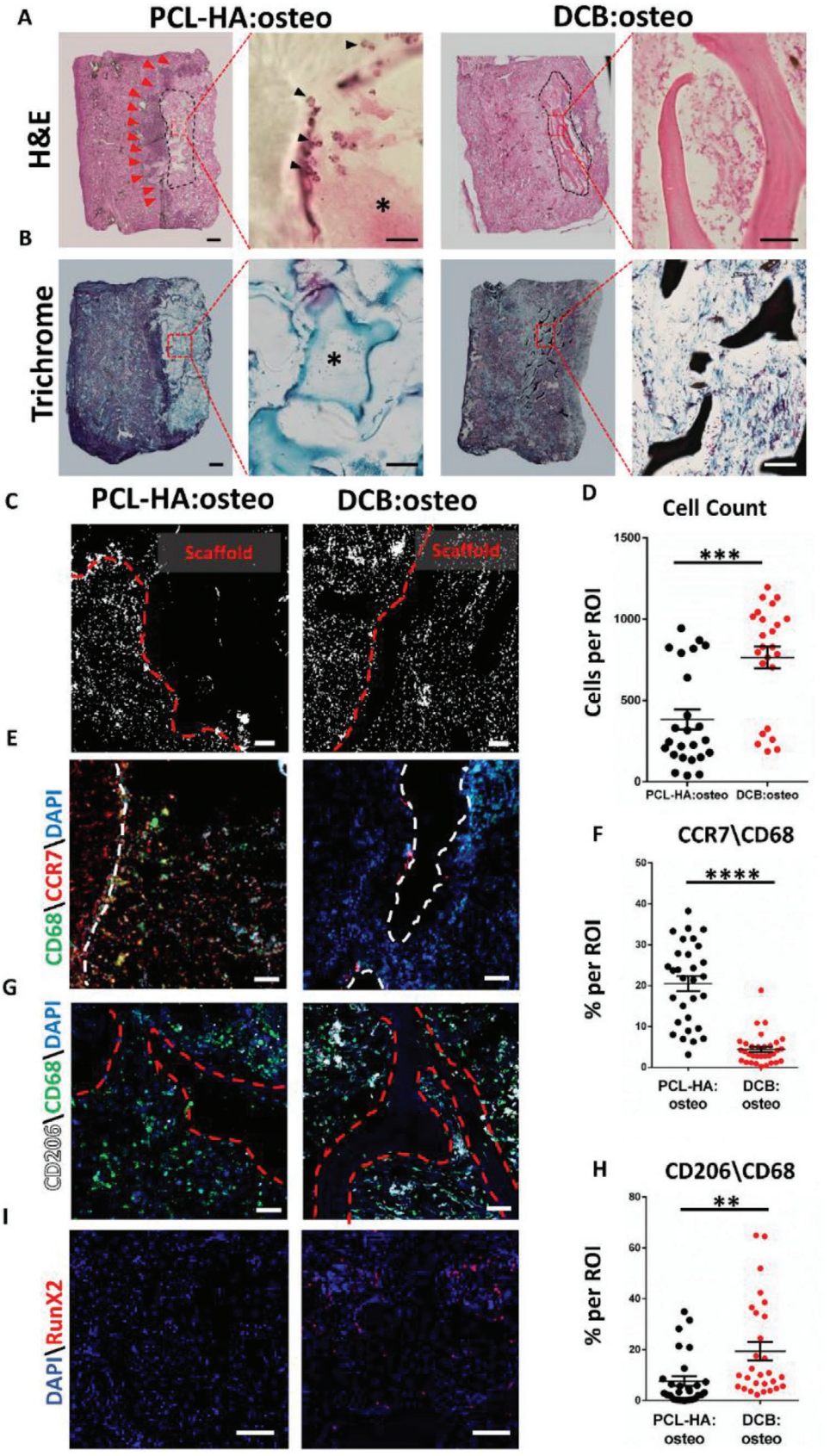

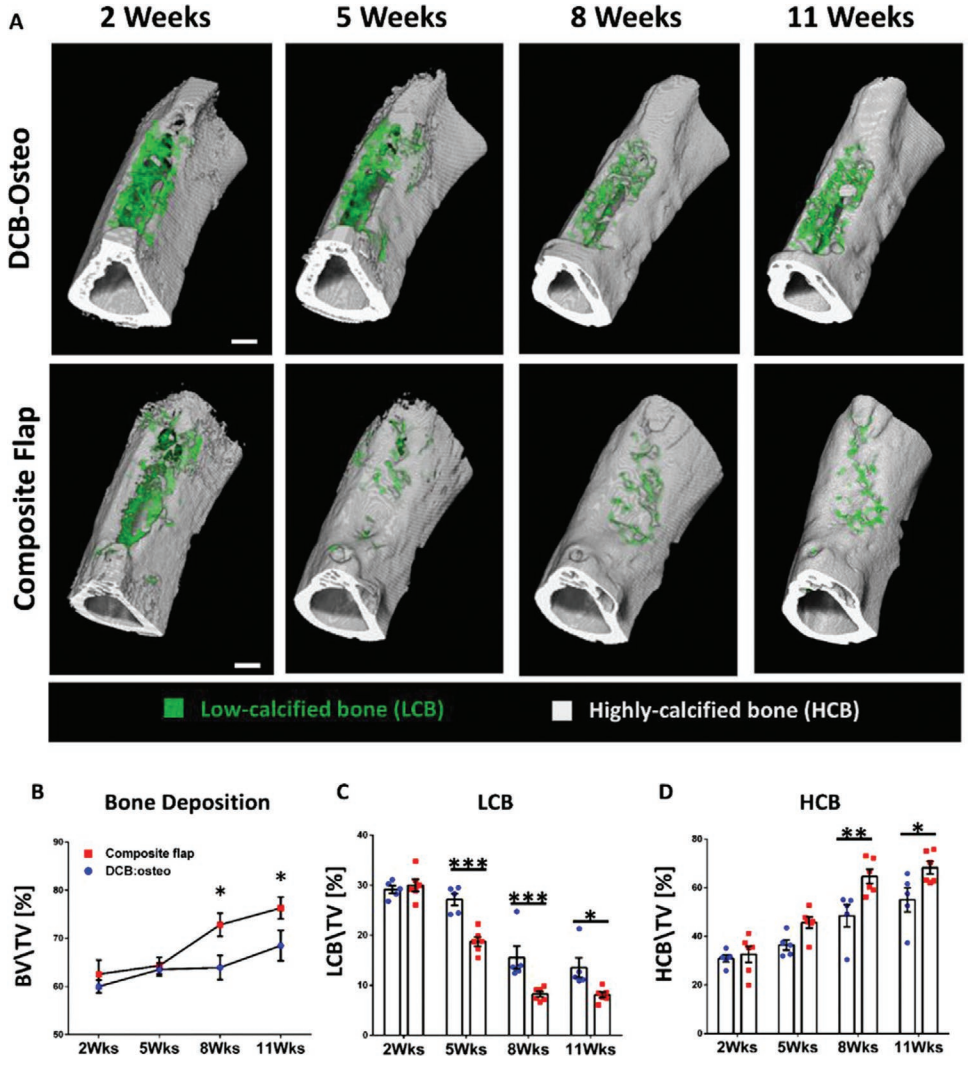

Figure 6. Engineered composite tissues utilized as surgical flaps support bone defect repair. A) Reconstructions of in vivo microCT scans at 2, 5, 8 and 11 weeks after surgery. Thresholded low-calcified (LCB) and highly calcified (HCB) mineralized tissues are represented by green and grey colors, respectively. Scale bar = 1 mm. B–D) In vivo longitudinal analysis of bone deposition (B, BV/TV), changes in LCB (C, LCB\TV) and HCB (D, HCB/TV) measured within defects. n = 5–6 animals per group, Results are presented as mean ± s.e.m (t-test). Significance levels: *$p < 0.05$, **$p < 0.01$,***$p < 0.001$.

rise was seen in both groups. However, while the percentage of HCB remained between 35% and 55% throughout the duration of the experiment in the DCB:osteo control group, composite flap treated defects contained >60% HCB by week 8 (Figure 6D). Defect filling rates indicated accelerated bone deposition between week 5 and 8 in the composite flap group as compared to the DCB:osteo only group, with all defects bridged by the end of week 8 (Figure S8B,C, Supporting Information).

2.6. Engineered Composite Tissues Support Bone Defect Vascularization and Soft Tissue Bridging

At the end of the experiment, rats were perfused with microfil contrast-agent to allow visualization and quantification of the blood supply in the defect area. X-ray scans of perfused hindlimbs revealed differences in blood capillary formation at the defect site. As expected, minimal capillary formation was evident outside of the cortical surface of defects repaired with

Figure 5. Use of a biological matrix in composite neo-tissues induces a favorable host response compared to synthetic scaffolds. A) H&E and B) trichrome stained tissue sections of composite tissues at 21 days post implantation; boxed areas are magnified. Red arrowheads outline dense hypercellular reactive layer in the PCL-HA:osteo group; black arrowheads mark multinucleated foreign body giant cells attached on inner PCL walls; asterisks mark low cellular content within scaffold spaces. Scale bars = 500, 100, and 20 µm. C,D) Segmentation of DAPI nuclear stain used to quantify cellular content within scaffold pores. Scale bar = 100 µm. E,G) Host's immune response assessed by co-labeling for CD68 (green, pan-macrophage marker), CCR7 (red, M1 inflammatory cells) and CD206 (white, M2 anti-inflammatory cells). Scale bar = 100 µm. F,H) Quantification of M1/CD68 (F) and M2/CD68 (H) ratios within scaffolds. I) Cellular content of DCB:osteo and PCL-HA:osteo scaffolds within composite tissues, stained for Runx2 cells after 21 days in vivo. Scale bar = 100 µm. $n = 4$ for animals per group for tissue section analysis, Results are presented as mean ± s.e.m (t-test). Significance levels: ** $p < 0.01$, ***$p < 0.001$, ****$p < 0.0001$.

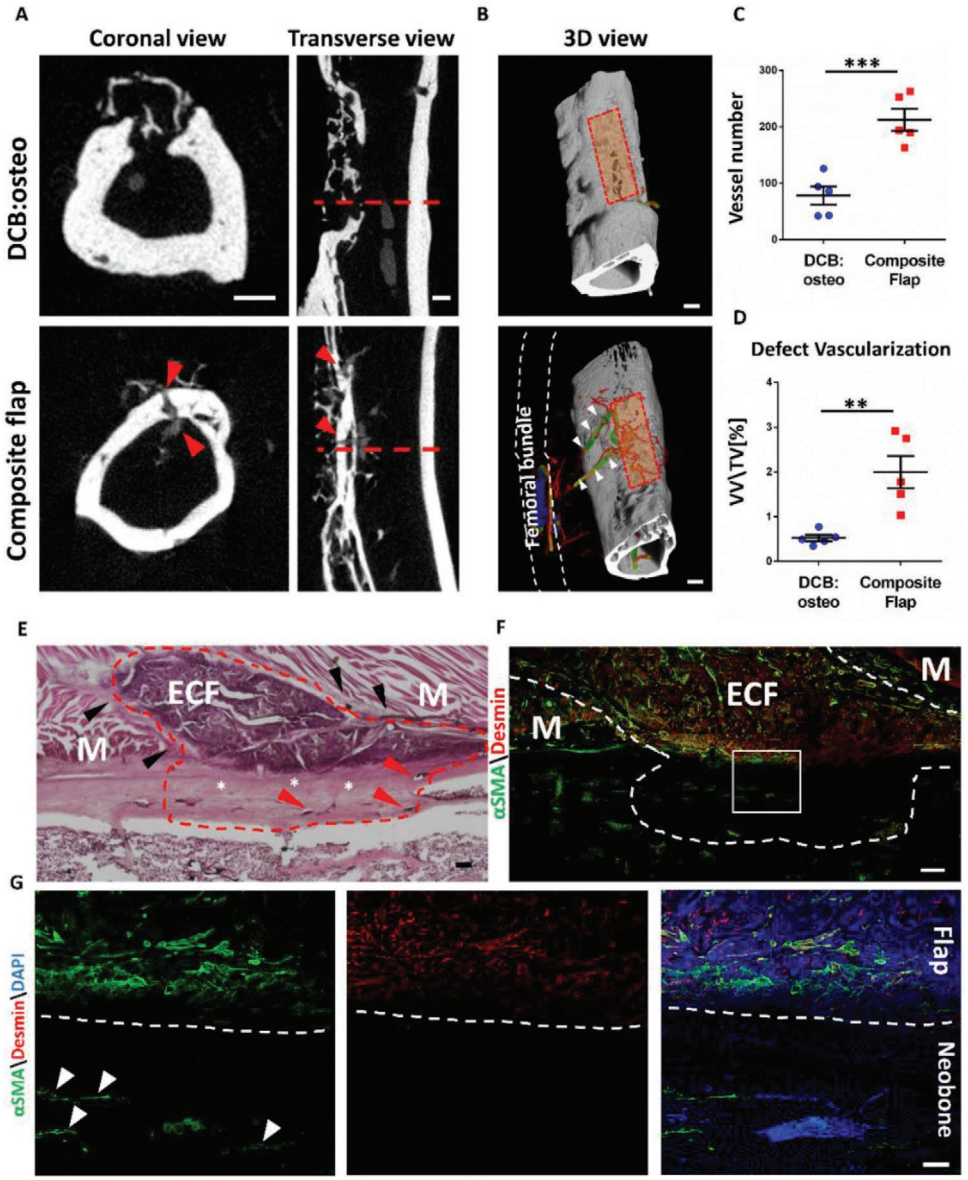

Figure 7. Engineered composite-tissue flap support bone defect vascularization and soft-tissue bridging. A) Representative coronal and transverse views of animal scanned at the end of the study, after perfusion with microfil contrast agent. Red arrowheads mark large penetrating vessels (150 µm> in diameter) through regenerated bone. Scale bar = 1 mm. B) 3D reconstruction of perfused samples. White arrowheads indicate vessels projecting from the femoral bundle through the composite tissues, toward regenerated bone (red dashed rectangle). C,D) Analysis of vessel volume within defects after 11 weeks (C) and number of vessels penetrating the neo-bone (D). E) H&E section of regenerated area at 11 weeks post-surgery, where a muscle defect was created in addition to the bone defect. Black arrowheads indicate muscle attachment to the engineered composite flap ("ECF"); red arrowheads indicate vessels within regenerated bone. Scale bar = 500 µm. F,G) Tissue section of regenerated defect immuno-labeled for α-SMA (green), desmin (red), and DAPI (blue); white dashed line delineates the engineered composite-tissue flap ("ECF") and regenerated bone, with host native muscles attached to the soft-tissue phase of the flap ("M"). G) Higher magnification of boxed region, with red dashed line indicating the composite tissue-neobone interface. White arrowheads mark α-SMA positive vessels within regenerated cortical region. Scale bars = 500, 100 µm. n = 5 animals per group. Results are presented as mean ± s.e.m (t-test). Significance levels: $^{**}p < 0.01$, $^{***}p < 0.001$.

DCB:osteo scaffolds alone (**Figure** 7A). In contrast, defects supported by composite flaps, featured a higher density of macro-vessels penetrating through the bridging bone, communicating between the medullary cavity and the outer surface of the tibia (Figure 7A,C). Vessels running from the major femoral vessels to the engineered tissue were visible in 3D reconstruction of specimens (Figure 7B). In general, a higher density of blood vessels was observed filling the tibial defects (Figure 7D). In animals bearing both a tibial and an 8 × 8 mm gracillis muscle defects, natural musculature had been re-attached to the soft phase of the engineered composite flap (Figure 7E). α-SMA was abundant in the composite flap indicating that it was well vascularized, and it was also visible in the regenerated bone supported by the engineered flap (Figure 7G). Moreover,

staining of muscle fibers was confined to the flap's soft-tissue phase attached to the outer surface of the tibia and adjacent native musculature (Figure 7G), with no traces detected within the bone defect.

3. Discussion

Composite-tissue flaps mobilized with an incorporated fully vascularized bone are routinely used for major reconstructions. To promote the survival and integration of the harvested bone, these flaps are harvested together with a rich vascular network that extends from the patients' circulatory system.[32–34] However, the harvest of autologous tissues has several limitations.[1,2]

While considerable work has focused on the composition, architecture, and biology of bone scaffolds to enhance vascularization,[21,30,35] only few studies have fabricated pre-vascularized TEBGs for live bone graft surgery[26,27,36] using autologous soft tissue to create a vascular pedicle for the bone scaffolds. In the current work, we have fabricated a composite neo-tissue flap, based on FDA approved biomaterials, to engineer vascularized soft-to-hard tissue constructs. After a 21-day incubation period, the formed composite-tissues were shown to integrate and vascularize in vivo. In addition, composite tissues were mobilized as flaps toward a tibial defect in rats, and in vivo scans were used to evaluate longitudinal bone repair. This methodology provides an effective alternative to standard practices of tissue harvest and vascular bone formation currently used for reconstructive surgery.

The composite flap in this work was based on initial pre-vascularization of soft-tissue matrices, using co-cultures of DPSCs and endothelial cells. DPSCs, an easily accessible population of resident progenitor cells that reside in the dental pulp cavity, are ectoderm-derived stem cells that express markers overlapping with MSCs.[37] This makes them a clinically relevant supportive cell niche for pre-vascularization purposes, with a well-documented pro-angiogenic effect on organization and engraftment of endothelial cells.[31,38–40] Recently, we have reported successful regeneration and re-vascularization of spinal cord injuries using the DPSC:HAMEC co-culture.[41] In the current work, bioengineered constructs based on DPSC:HAMEC co-cultures were implanted in a femoral AV bundle model, and incorporated together with a decellularized bone. Pre-vascularized implants were associated with robust vascular organization in vivo. This finding is in line with previous reports of the outcome of vessel-bearing soft tissue and organ implants,[14,28,42] where capillary invasion and tissue function were positively affected by pre-vascularization. In remodeled pre-vascularized constructs, which served as vascular conduits for decellularized bone in vivo, close interaction between host and graft ECM components was evident. Vessel-supporting structures may have played a critical role during tissue formation. In prevascularized specimens 21 days after initial implantation, laminin fibers originating from bioengineered constructs were co-labeled with host capillaries (Figure 2). Laminin, a pivotal component in developing capillaries, may have maintained vessel stability during host tissue remodeling.[43,44] Other implant-associated vascular components shown to survive transplantation were elastin and collagen IV, known to promote neo-vessel elongation and survival.[45,46] Thus, implanted matrix components appeared to play a critical role in guiding and supporting neo-vessel penetration and remodeling within the forming composite tissues. The ECM components were mediating host and graft connectivity and development. Vascular remodeling of bioengineered constructs by hosts was demonstrated by co-labeling of the engineered vessels and invading capillaries (Figure S2, Supporting Information). These observations resonate with published data from studies in which organized pre-vascularized matrices underwent rapid replacement by host vasculature in vivo.[15,47]

A limited number of published studies have focused on neo-fabrication of soft-tissue pedicles for vascular support of bone biomaterials. Several groups induced bone scaffold vascularization by direct incorporation of a vascular bundle within the implanted biomaterial.[48,49] While these procedures promote vessel sprouting and subsequent bone formation within the bone construct, further utilization of the integrated scaffold for defect repair remains limited. Cai et al.[26] implanted coral hydroxyapatite (CHA) scaffolds seeded with bone marrow MSCs, within the spatium intramuscular of beagle dog subjects. After 4 weeks of in vivo maturation, a second surgery was performed in which the saphenous vessels were ligated, followed by axial rotation of the harvested muscle pedicle with exposed CHA scaffold to an orthotopic site. Fan et al.[36] incorporated β-tricalcium phosphate (β-TCP) scaffolds together with the saphenous vessels and a fascia flap to repair tibial defects in rhesus monkeys. In both studies, mineral deposition, and vessel penetration within defect were shown to be optimal in cell-seeded bone scaffolds, supported by a vascular network. While these and other studies have shown impressive progress in bone regeneration using large animal models, they rely on soft-tissue harvest for bone vascularization and mobilization. One of the most frequently harvested tissue is the latissimus dorsi muscle,[50,51] which has been associated with complications such as post-operative pain.[52] Moreover, soft-tissue repair has not been achieved in these studies, and in many clinical settings, large soft-tissue defects accompany bony defects, making proper closure and repair a challenging task. In the present study, the vascularized soft-tissue portion of the newly formed flap is the result of pre-vascularized biomaterial remodeling. Neo-tissues engulfed the bones (Figure 2) fully supported by a newly formed functional vascular tree that was visualized by high-resolution microCT (Figure 4).

Decellularized bovine trabecular bone has been approved for clinical use as bone reconstruction material, with products including Cancello-Pure and CopiOs bone wedges that are commercially available. The lack of immunogenicity has been demonstrated in numerous animal implantation studies, as decellularization removed all cellular material from the bone.[53–55] While human bone matrix would be ideal for engineering new bone, the availability and consistency of bovine bone, along with effective decellularization and rigorous quality control made it a material of choice for many clinical applications. Another advantage of bovine bone matrix is a close resemblance to human bone. Our group has conducted several studies of bone and osteochondral tissue regeneration in

a human-sized porcine model of orthotopic implantation using decellularized bovine bone as a scaffold.[12,56] This technology is now entering clinical studies by epiBone.

Osteogenic induction of DCBs, achieved by seeding and differentiating mesenchymal stromal cells within scaffold pores, has proven to be beneficial for maturation and regeneration of bioengineered bone even in clinically applicable models.[11,12,27,57] Adipose-derived mesenchymal stromal cells were used for DCB seeding in vitro, as they are extremely advantageous in clinical settings, owing to their easy harvesting from lipoaspirates and the potential for large-scale expansion and multi-lineage differentiation.[58,59] At the end of the 21-day incubation period, cells were filling interior pore spaces with newly secreted mineral and osteogenic ECM (Figure 3; Figure S3, Supporting Information). After formation of neo-tissues with either acellular or osteogenically induced DCBs, inspection of composite tissues revealed major differences in vascular organization. Histological and microCT-based evaluations found an abundance of mature penetrating vessels within DCB:osteo constructs (Figures 3,4), with Runx2-positive cells in proximity to neo-capillaries in DCB:osteo scaffolds (Figure S4, Supporting Information). During post-natal bone development and repair, angiogenesis and osteogenesis are two closely associated processes. Amongst other cell types, osteoblasts are a major source of pro-angiogenic factors which initiate endothelial cell activation.[60] Endothelial cells in turn have been shown to influence bone homeostasis and osteogenesis in several ways, including the formation of type-H vascular-niches that promote osteoblast accumulation and function[61] or via paracrine effects, such as Notch and Noggin signaling.[62] In the current study, osteogenically committed MSCs, engineered endothelial structures and penetrating host capillary plexus were collectively organized within composite tissues. The synergistic effect of these cellular systems could promote positive feedback between upregulation, recruitment and differentiation of host cells while continuously enhancing capillary formation. However, these mechanisms require further examination in subsequent studies.

The decellularized bones used in the current study outperformed synthetic PCL-based bone scaffolds. While vascularization, tissue penetration and host immune response were favorable in bioengineered constructs made using bone matrix, an adverse immune reaction developed in constructs made using PCL scaffolds (Figure 5; Figures S6 and S7, Supporting Information). One possible reason for this outcome is the implantation and integration of bone scaffolds (either DCBs or PCL) within an engineered soft-tissue, which is not an autologous tissue. This may have augmented the host immune response which could be dynamically different than foreign body reactions documented in subcutaneous implantation models. Owing to its biocompatibility, controllable degradation rate and accurate patient-specific fabrication, PCL is considered a pivotal biomaterial in the field of bone tissue engineering.[63–65] Further research should focus on immunomodulatory approaches to advance the use of synthetic materials, particularly, but not limited to PCL, in the suggested composite tissues.

To highlight the regenerative capacity of composite neo-tissues, we used engineered flaps to support 5-mm long monocortical defect repair. Here, contributing vessels from neo-tissue flaps were volumetrically quantified and shown to outnumber vessels in controls unsupported by flaps. In the study by Wang et al., rabbit femoral defects supported by vascular pedicles were affected in a similar manner. Bone scaffolds exhibited higher numbers of penetrating vessels as well as increased VEGF levels within regenerated defects, in contrast to the scaffold-only control group.[27] During bone engraftment, the composite-flap's vascular niche may have led to localized elevated VEGF levels in the bone defect. VEGF is a pivotal factor in initiating early angiogenesis, and is also found in proliferating osteoblasts within bone osteotomies.[66,67] Moreover, it can aid to indirect bone formation by increasing local circulation and vascular permeability, ultimately enhancing the accessibility of circulating cells that contribute to ongoing bone repair, to the implantation site.[68,69] The deposited bone in the current study continuously filled defects with higher turnover of hypodense bone, toward a more mineralized content in the composite-flap group compared to DCB:osteo controls (Figure 6; Figure S8, Supporting Information), supporting the notion that vessels originating from engineered flaps physically supported the recruitment of host cells,[70] and provided vascular feeding of engrafted bone.[71] As for implanted MSCs, remnants of human nucleic acids were identified within the neo-bone 11 weeks after bone surgeries (Figure S9, Supporting Information). As described above and previously shown by others[72,73] transplanted MSCs may have had a transitional role during bone remodeling within flaps (Figure 3; Figure S4, Supporting Information) and subsequent defect repair.

Bridging the soft- and hard-tissue defects was an additional issue we set to resolve. An osteomuscular defect was created by partial dissection of the gracillis muscle together with the bony defect (Figure 7). The remaining musculature was re-attached to the soft portion of the exposed composite flap. Numerous studies have focused on strategies for either bone[74,75] or muscle[76,77] biomaterial-based repair, while the focus of studies involving soft-to-hard multi-phased grafts remains on interface tissue engineering, namely osteochondral[78] and ligament-to-bone tissue constructs.[79,80] We also attempted to bridge an osteomuscular defect. 11 weeks after injury, the bony defect was bridged with cortical bone, with continuous attachment of the engineered flaps to the outer surface of the tibial diaphysis and neighboring musculature. The composite neo-tissue was well vascularized, as evident from α-SMA labeling, which was also evident in the vasculature within the neo-bone. Desmin staining confined within the attached flap verified that muscle fibers were organizing in the neo-tissue without soft-tissue prolapse into the bone defect (Figure 7). Further attempts to study the nature of muscle repair could be made using this model, by adding a niche within the forming neo-tissues which favors muscle fiber regeneration and penetration from neighboring tissues.[4] Future studies should also set to repair large load-bearing bone defects. Upscaling the composite tissue and moving onto large animal models will help in addressing clinically relevant challenges.

4. Conclusion

The current work demonstrated the formation of composite tissues, comprising an engineered vascular pedicle that engulfs

and vascularizes a decellularized bone. By using these neo-tissues as axially rotated flaps for a live bone graft surgery model, vascularization and osteogenesis in a tibial defect were significantly elevated. The proposed approach may provide an opportunity to develop new tissue replacements, making extensive autologous tissue harvest obsolete.

5. Experimental Section

Cell Culture: Human adipose microvascular endothelial cells (HAMECs Passage 7-8, ScienceCell) were lentiviral-transduced with ZsGreen fluorescent protein and cultivated in endothelial cell medium (ScienceCell) supplemented with 5% fetal bovine serum (FBS) (ScienceCell) and endothelial cell growth supplement (ScienceCell). Adipose-derived MSCs (Passage 5-6, Lonza) were cultured in Dulbecco's modified Eagle medium (DMEM, Gibco), supplemented with 10% FBS (HyClone), 1% Glutamax (Gibco), and 1% penicillin-streptomycin solution (Biological Industries). For osteogenic differentiation, an osteogenic differentiation medium was used containing low-glucose DMEM (Gibco), 10 nm dexamethasone (Sigma), 10 mM sodium-β-glycerophosphate (Sigma), 0.88 mg mL^{-1} ascorbic acid (Sigma), 1% penstrep (Biological industries), and 10% FBS (HyClone). Cellular commitment toward osteogenic differentiation was confirmed with alizarin staining (ScienCell). Dental pulp stem cells (DPSCs, passage 7-8, Lonza) were grown in low-glucose DMEM (Gibco) supplemented with 10% FBS (HyClone), 1% nonessential amino acids (Gibco), 1% Glutamax (Gibco), and 1% penicillin-streptomycin nystatin solution (Biological Industries).

Soft-Tissue Construct Preparation: 3D scaffolds were prepared using the particle leaching technique.[81] PLLA/PLGA polymer solution (0.7 mL) was prepared from a 1:1 mixture of a 50% PLLA (Polysciences) solution and 50% PLGA (Boehringer Ingelheim) solution, dissolved in chloroform. 0.7mL of the homogeneous solution was added to 1.17 g of sodium chloride particles maintained in Teflon molds. After evaporation, salt particles entrapped in scaffolds were dissolved by deionized water washes, resulting in interconnected pores (pore size ranging from 212–600 μm).

Soft-Tissue Constructs Pre-Vascularization: PLLA/PLGA scaffolds were seeded with either a DPSC:HAMEC co-culture (3:1 ratio) or HAMECs only (control). Scaffolds were sterilized in ethanol, washed, and dried prior to cell loading. Cells were trypsinized and resuspended in a 1:1 mixture of thrombin/fibrinogen solution (Evicell) and seeded onto 10 × 22 mm rectangular PLLA/PLGA scaffolds at a seeding density of 5.5 × 10^3 mm$^{-2.}$ After 30 min in a humidified chamber, either DPSC:HAMEC (1:1) or HAMEC medium was added to the constructs. Scaffolds were incubated for 1 week, with a medium change every 48 h, until implantation.

Hard-Tissue Scaffold Preparation: Both decellularized bone and polycaprolactone (PCL) scaffolds were prepared using previously published protocols,[12,82,83] with some modifications.

For bone scaffolds, blocks of cancellous bone, 4 cm in diameter and 7 cm long, were created from the distal aspect of adult bovine femurs (>2 years old animals) using a 44-mm diameter, 75-mm long hole saw (PipeMan Products, Inc.) attached to a hammer drill (Bosch). These cores were milled into the 2.5 by 5.5 mm cylindrical scaffolds. The scaffolds were stripped of all cellular material to leave behind only the mineralized ECM with largely preserved composition, architecture, and mechanical properties using the previously established protocol.[11,12,84] The bone was washed with high-velocity streams of water to remove the marrow from the pore spaces, and treated on an orbital shaker in four steps to remove any remaining cellular material: i) PBS with 0.1% EDTA (w/v) for 1 h at room temperature; ii) hypotonic buffer (10 mM Tris, 0.1% EDTA (w/v) in DI water) overnight at 4 °C; iii) detergent (10 mM Tris, 0.5% SDS (w/v) in DI water) for 24 h at room temperature; iv) enzymatic solution (100 U mL^{-1} DNase, 1 U mL^{-1} RNase, 10 mM Tris in DI water) for 6 h at 37 °C. Decellularized bone blocks were freeze-dried, subjected to sonication treatment to remove any remaining debris, and stored in 70% ethanol (v/v) under UV for sterilization. Prior to cell seeding, the scaffolds were washed and submerged in DMEM overnight.

For PCL scaffolds, cylindrical sacrificial molds were designed using Solidworks, and CAD models were printed using sacrificial material (BVOH, Verbatim) on an i3 MK2.5 desktop printer (Prusa) modified with a 0.25 mm nozzle. Molds were printed using a rectilinear pattern with a 60% printing density. PCL (Polyscience Cat26289) was dissolved in chloroform and hydroxyapatite (HA) particles (Sigma Cat677418) were added to the solution (10% [w/w] of PCL, Sigma) which was subjected to three 15 min cycles of sonication to break up mineral aggregates. The resulting PCL-HA solution was briefly vortexed and cast into sacrificial molds. These were then subjected to two cycles of centrifugation and left in a ventilated hood to allow for solvent evaporation. After 24 h at room temperature, dried molds containing the polymer were washed in deionized water and templates were dissolved, yielding PCL-HA cylindrical scaffolds 5.5 mm in length and 2.5 mm diameters.

Osteogenic Induction of Hard-Tissue Scaffolds: Human adipose derived MSCs were expanded in T-75 tissue flasks until 80–90% confluency. At the day of seeding, cells were trypsinized and loaded onto cylindrical DCBs or PCL-HA scaffolds using a 1:1 mixture of thrombin/fibrinogen solution (Evicell) at a cellular density of 15 × 10^3 cells mm^{-2}. After cellular attachment onto scaffolds, MSCs cultivation medium was added for 48 h, after which it was replaced with osteogenic differentiation medium which was changed every 48 h for a period of 21 days. Induced DCBs and PCL-HA were termed DCB:osteo and PCL-HA:osteo respectively.

Implantation of Composite Tissue Constructs: All animal experiments were approved and conducted under the supervision of the Technion Pre-Clinical Research Authority (PCRA Technion, approval ethics no. 177-12-17). 3 days prior to implantation, rats received a daily dose cyclosporine administered subcutaneously (10 mg kg^{-1}). On the day of surgery, rats were anesthetized using 3% isoflurane inhalation. Under sterile conditions hard-tissue scaffolds were carefully divided into thirds using sterile scalpel and under magnification and kept in a humidified chamber until implanted. Rats' lower hindlimbs were draped and cleaned, and an incision was made medial to the tibial crest on the ventral side of the lower hindlimb. The tibial branch of the femoral AV bundle was carefully exposed distally to the knee joint and proximally to the bifurcation. Bioengineered soft-tissue constructs were positioned under the exposed vessels, followed by attachment of the bone scaffold using a 1:1 mixture of thrombin/fibrinogen solution (Evicell). Soft-tissue constructs were wrapped around the exposed bundle with their ends joined using 8-0 silk sutures. Sterile nitrile was used to isolate the graft from adjacent soft tissues and skin and secured with 6-0 nylon sutures. The overlying fascia and skin were sutured layer-by-layer, using 5-0 absorbable sutures. After the procedure, buprenorphine was administered subcutaneously (0.03 mg kg^{-1} body weight). Animals recovered in an oxygenated cage on a heating pad and were monitored daily, for 21 days. After 21 days, rats were either euthanized and explanted neo-tissues used for analysis, or neo-tissues were exposed and used as reconstruction tissue-flaps for bone defects.

Tissue Defect and Composite Flap Rotation Procedure: On the day of surgery, rats were anesthetized using 3% isoflurane inhalation. After separation of the tibialis anterior and gracillis muscles, the tibial crest was exposed and a monocortical 2 ×2 × 5 mm defect was created using a diamond burr, with constant irrigation. In the control group, a DCB:osteo scaffold was press-fitted into the defect. The defect was covered with sterile nitrile rubber, separating it from adjacent soft tissues. In the treatment group where a 21-day old composite flap had formed, the femoral AV bundle with the engineered tissue were re-exposed from the level of the inguinal ligament and proximal to the tibial and peroneal AV bifurcation. The outer surface of the embedded DCB:osteo was partially exposed using a sterile scalpel to allow direct scaffold-to-bone contact within the defect. The distal end of the femoral bundle was ligated with 4-0 silk sutures to facilitate axial tissue transfer of the composite tissue as a flap toward the bone defect. Exposed DCB was press-fitted into the tibial defect and sterile nitrile rubber was used to cover the transferred tissue. At the end of the procedure, overlying

fascia and skin were sutured layer-by-layer, using 5-0 absorbable sutures. Animals recovered in an oxygenated cage on a heating pad and were monitored daily; buprenorphine was administered subcutaneously for 3 days (0.03 mg kg^{-1} body weight). Daily cyclosporine subcutaneous injections (10 mg kg^{-1} body weight) were administered for the full duration of the experiment.

Pre-Implantation Assessment of Cytokine Secretion: Medium was collected from seeded constructs, 3 and 7 days after seeding. The Human Angiogenesis Array (RayBiotech, GSH-ANG-1-1) was used to assess secretion of Ang2 and VEGF. Fluorescence was read using the GenePix Microarray, at an emission wavelength of 570 nm. Human ANGPT1 ELISA (RayBiotech, ELH-Angiopoietin1-1) was used for Ang1 quantification. Absorbance was measured at 450 nm, using a microplate reader.

Confocal Imaging of Pre-Implanted Soft-Tissue Constructs: 3 and 7 days after seeding, scaffolds were imaged under a Zeiss LSM700 inverted confocal microscope (Carl Zeiss). Average vessel length, total vessel length and vessel area within the constructs were calculated by analyzing z-stack confocal projection images, using the AngioTool software.

Whole-Mount Staining of Soft-Tissue Constructs: After 7 days of incubation, scaffolds were fixated in 4% paraformaldehyde for 20 min, followed by permeabilization in 0.3% Triton x-100 (Bio Lab Ltd.) and blocking in 5% BSA solution (Millipore). Samples were then incubated with the following primary and secondary antibodies: mouse anti human collagen type IV (1:500, Sigma, C1926), mouse anti human elastin (1:1000, E4013, Sigma), mouse anti human laminin (Dako M0638), and donkey anti-mouse Alexa-647 (1:400, Jackson 715-605-151) mixed with DAPI (1:1000, Sigma) in PBS, for 2 h, at room temperature.

Laser Speckle Contrast Imaging of 21 Days Old Composite Tissues: On day 21 post-implantation, animals were anesthetized with 3% isoflurane inhalation. Grafts were exposed and imaged using an FLPI-2 laser speckle contrast imager (Moor Instruments Inc., DE, USA). Three consecutive exposures lasted 10 s each, at 752 × 580-pixel resolution. For each graft, the imaging process yielded both a color image and a corresponding perfusion-flux image. Images were exported and analyzed using the moorFLPI-2 Measurement V1.0 software. Color images were used to delineate the total outline and lateral thirds were used for flux analysis, excluding readings originating from the femoral bundle.

MicroCT Angiography of Bioengineered Composite Tissues: 21 days after implantation, rats were euthanized using CO_2 inhalation, and transcardially perfused with 60 mL warm heparinized saline. Thereafter, 15 mL freshly prepared silicone rubber contrast agent (Microfil, MV-122, FlowTech Inc., Carver, MA) was infused. Microfil solution was allowed to polymerize at 4 °C overnight, after which the grafts were harvested and immersed for 20 min in 4% PFA solution. Explants containing the cast of the vascular tree were scanned using a high-resolution microCT scanner (Skyscan 1276, Bruker, Kontich, Belgium) with both bone and contrast agent intact. Explants were then gently decalcified overnight at 4 °C, with 0.5 M EDTA (Sigma), after which scans were repeated under the same parameters and co-registration-based subtraction was performed to distinguish implanted bone scaffolds from perfused microvasculature. The following scanning parameters were used: source voltage of 55 kV, source current of 72 µA, applied filter of aluminum 0.25 mm using a 0.2° rotation step. Image acquisition was performed with a scaled pixel size of 10 µm.

In Vivo MicroCT: In vivo x-rays and microCT scans were performed at 2, 5, 8, and 11 weeks post-surgery to assess bridging and follow bone deposition within defects. Prior to scans, rats were anesthetized using 3% isoflurane inhalation and treated hindlimbs were stabilized, as previously described[85] prior to scanning. In vivo scans were performed using a high-resolution in vivo scanner (Skyscan 1276, Bruker, Kontich, Belgium) with an applied Al-Cu filter at 80 kV, 120 µA, and 21 µm voxel size. Scan duration was ≈11 min and yielded 600 projections at 360°.

Construction of 3D Models, Morphometry, and Analysis: Back projections were reconstructed using NRecon (Skyscan, version 1.7.2.0). 287 sections containing a 2 × 2× 6 mm rectangular volume of interest were analyzed with a combined adaptive and global threshold to calculate BV/TV values as well as to differentiate between deposited low-calcified bone (LCB) and highly calcified bone (HCB). Dataviewer (Skyscan, version 1.5.4.6) was used for co-registration of multiple scans, CTAnn Software (Skyscan, version 1.17.7.2) was used for segmentation, VOI for construction and analysis, and CTVox (Skyscan, version 2.2.0) was for 3D visualization.

Histology and Immunofluorescence: For pre-implantation immunofluorescence, scaffolds were fixated in 4% PFA for 20 min, decalcified for 24 h, at 4 °C using EDTA 0.5 M (Sigma), washed and embedded in optimal cutting temperature compound (TissueTek) and frozen at −20 °C for cryosectioning (20 µm). Sections were permeabilized with 0.5% Tween solution, washed, blocked with 5% BSA and incubated overnight with the following antibodies: Runx2 (1:100, Santa Cruz, SC-390351), rabbit anti-collagen type1 (1:200, Abcam, ab34710), rabbit anti-BSP2 (1:1000, Millipore, AB1854) and labeled with donkey anti-mouse Alexa-647 (1:400, Jackson 715-605-151), donkey anti-rabbit Cy3 (1:400, Jackson, 715-605-152) mixed with DAPI (1:1000, Sigma) in PBS, for 2 h, at room temperature.

For 21-day-old composite tissues as well as whole tibia explants, decalcification was either performed overnight at 4 °C, or for 2 weeks at 37 °C, using EDTA 0.5 M (Sigma), with gentle agitation. Explants were prepared for sectioning according to published protocols.[86] Briefly, tissues were immersed overnight in a cryoprotectant solution (20% sucrose, 2% PVP), embedded in a compound comprised of 20% sucrose, 2% PVP (Sigma) and 8% gelatin (Sigma), and frozen at −80 °C for cryosectioning (5 or 20 µm thick). H&E and trichrome stains were used for general assessment of construct remodeling and host reaction. For immunostaining, tissue sections were incubated in 0.5% Tween solution for 20 min, rinsed with PBS and blocked with 5% BSA (Millipore), for 1 h, at room temperature, followed by overnight incubation at 4 °C with antibodies for the following markers: CD68 (1:50, Serotec, MCA341R) as a pan-macrophage marker; CCR7 (1:100, Abcam, ab32527) and CD206 (1:1000, Abcam, ab64693) as M1 and M2 macrophage markers, respectively; anti rat CD31 (1:100, BD-Science, 550300), anti-human CD31 (1:50, Abcam, ab28364), laminin (1:200, Abcam, ab11575) and anti α-SMA (1:100, Abcam, ab5694) were used for visualization of neo-vasculature and mural cells within composite tissues. Desmin (SC-7559) was used to evaluate muscle fibers organization and anti-human nucleic acid (1:50, Merck, MAB1281) was used to label tranplanted cells. Sections were labeled with DAPI (1:1000, Sigma), donkey anti-mouse Alexa-647 (1:400, Jackson 715-605-151), and donkey anti-rabbit Cy3 (1:400, Jackson, 715-605-152) mixed with DAPI (1:1000, Sigma) in PBS, for 2 h, at room temperature.

Statistical Analysis: Quantitative results were obtained from at least three independent samples for in vitro and at least five samples from rat in vivo experiments. Statistical analyses were performed using GraphPad Prism 7 and Matlab. Single comparisons were made with Student's *t*-test. To examine differences between multiple groups, one-way or two-way analysis of variance (ANOVA) was performed, with post-hoc Tukey's multiple comparisons. All data are presented as mean ± SEM; significance levels: ns = non-significant, $*p < 0.05$, $**p < 0.01$, $***p < 0.001$, $****p < 0.0001$.

Supporting Information

Supporting Information is available from the Wiley Online Library or from the author.

Acknowledgements

This project has received funding from the European Research Council (ERC) under the European Union's Horizon 2020 Research and Innovation Programme (grant agreement no. 818808), and was supported by the Israel Science Foundation (ISF grant no. 1421/16) and NIH (grant no. EB027062). The authors thank the Technion's Pre-clinical Research Authority and Mark Tendler for the assistance with animal care. The author thank Dr. Edith Suss-Toby and Dr. Esther Messer from the Technion's BCF staff and Dr. Phil Salmon from Bruker-Skyscan for their advice on microCT

studies. The authors also thank Janette Zavin for histological processing, and Dr. Yehudit Posen and Dr. Dina Safina for proofreading the article.

Conflict of Interest

The authors declare no conflict of interest.

Data Availability Statement

The data that support the findings of this study are available from the corresponding author upon reasonable request.

Keywords

composite tissues, decellularized bones, live bone grafts, osteogenesis, reconstruction flaps, tissue engineering, vascularization

Received: October 12, 2020
Revised: January 7, 2021
Published online:

[1] P. V. Giannoudis, H. Dinopoulos, E. Tsiridis, *Injury* **2005**, *36*, S20.
[2] R. Dimitriou, E. Jones, D. McGonagle, P. V. Giannoudis, *BMC Med.* **2011**, *9*, 66.
[3] E. S. Place, N. D. Evans, M. M. Stevens, *Nat. Mater.* **2009**, *8*, 457.
[4] M. Zhu, W. Li, X. Dong, X. Yuan, A. C. Midgley, H. Chang, Y. Wang, H. Wang, K. Wang, P. X. Ma, D. Kong, *Nat. Commun.* **2019**, *10*, 4620.
[5] T. Lin, S. Liu, S. Chen, S. Qiu, Z. Rao, J. Liu, S. Zhu, L. Yan, H. Mao, Q. Zhu, D. Quan, X. Liu, *Acta Biomater.* **2018**, *73*, 326.
[6] G. M. Cunniffe, P. J. Diaz-Payno, E. J. Sheehy, S. E. Critchley, H. V. Almeida, P. Pitacco, S. F. Carroll, O. R. Mahon, A. Dunne, T. J. Levingstone, C. J. Moran, R. T. Brady, F. J. O'Brien, P. A. J. Brama, D. J. Kelly, *Biomaterials* **2019**, *188*, 63.
[7] Y. Gu, J. Zhu, C. Xue, Z. Li, F. Ding, Y. Yang, X. Gu, *Biomaterials* **2014**, *35*, 2253.
[8] J. L. Dziki, L. Huleihel, M. E. Scarritt, S. F. Badylak, *Tissue Eng., Part A* **2017**, *23*, 1152.
[9] A. H. Morris, D. K. Stamer, T. R. Kyriakides, *Semin. Immunol.* **2017**, *29*, 72.
[10] G. S. Hussey, J. L. Dziki, S. F. Badylak, *Nat. Rev. Mater.* **2018**, *3*, 159.
[11] W. L. Grayson, M. Fröhlich, K. Yeager, S. Bhumiratana, M. E. Chan, C. Cannizzaro, L. Q. Wan, X. S. Liu, X. E. Guo, G. Vunjak-Novakovic, *Proc. Natl. Acad. Sci. USA* **2010**, *107*, 3299.
[12] S. Bhumiratana, J. C. Bernhard, D. M. Alfi, K. Yeager, R. E. Eton, J. Bova, F. Shah, J. M. Gimble, M. J. Lopez, S. B. Eisig, V.-N. Gordana, *Sci. Transl. Med.* **2016**, *8*, 343ra83.
[13] F. A. Auger, L. Gibot, D. Lacroix, *Annu. Rev. Biomed. Eng.* **2013**, *15*, 177.
[14] S. Ben-Shaul, S. Landau, U. Merdler, S. Levenberg, *Proc. Natl. Acad. Sci. U. S. A.* **2019**, *116*, 2955.
[15] L. Perry, S. Landau, M. Y. Flugelman, S. Levenberg, *Commun. Biol.* **2018**, *1*, 161.
[16] U. Kneser, L. Stangenberg, J. Ohnolz, O. Buettner, J. Stern-Straeter, D. Möbest, R. E. Horch, G. B. Stark, D. J. Schaefer, *J. Cell. Mol. Med.* **2006**, *10*, 695.
[17] M. K. Smith, M. C. Peters, T. P. Richardson, J. C. Garbern, D. J. Mooney, *Tissue Eng.* **2004**, *10*, 63.
[18] R. E. Unger, S. Ghanaati, C. Orth, A. Sartoris, M. Barbeck, S. Halstenberg, A. Motta, C. Migliaresi, C. J. Kirkpatrick, *Biomaterials* **2010**, *31*, 6959.
[19] U. Utzinger, B. Baggett, J. A. Weiss, J. B. Hoying, L. T. Edgar, *Angiogenesis* **2015**, *18*, 219.
[20] J. Folkman, M. Hochberg, *J. Exp. Med.* **1973**, *138*, 745.
[21] M. I. Santos, R. L. Reis, *Macromol. Biosci.* **2010**, *10*, 12.
[22] J. T. Borenstein, E. J. Weinberg, B. K. Orrick, C. Sundback, M. R. Kaazempur-Mofrad, J. P. Vacanti, *Tissue Eng.* **2007**, *13*, 1837.
[23] U. Kneser, E. Polykandriotis, J. Ohnolz, K. Heidner, L. Grabinger, S. Euler, K. U. Amann, A. Hess, K. Brune, P. Greil, M. Stürzl, R. E. Horch, *Tissue Eng.* **2006**, *12*, 1721.
[24] O. Scheufler, D. J. Schaefer, C. Jaquiery, A. Braccini, D. J. Wendt, J. A. Gasser, R. Galli, G. Pierer, M. Heberer, I. Martin, *J. Cell. Mol. Med.* **2008**, *12*, 1238.
[25] E. Polykandriotis, A. Arkudas, R. E. Horch, M. Stürzl, U. Kneser, *J. Cell. Mol. Med.* **2007**, *11*, 6.
[26] L. Cai, Q. Wang, C. Gu, J. Wu, J. Wang, N. Kang, J. Hu, F. Xie, L. Yan, X. Liu, Y. Cao, R. Xiao, *Biomaterials* **2011**, *32*, 8497.
[27] L. Wang, H. Fan, Z. Y. Zhang, A. J. Lou, G. X. Pei, S. Jiang, T. W. Mu, J. J. Qin, S. Y. Chen, D. Jin, *Biomaterials* **2010**, *31*, 9452.
[28] R. Mishra, B. M. Roux, M. Posukonis, E. Bodamer, E. M. Brey, J. P. Fisher, D. Dean, *Biomaterials* **2016**, *77*, 255.
[29] L. Chen, Q. Xing, Q. Zhai, M. Tahtinen, F. Zhou, Y. Xu, S. Qi, F. Zhao, *Theranostics* **2017**, *7*, 117.
[30] G. D. Barabaschi, V. Manoharan, Q. Li, L. E. Bertassoni, *Adv. Exp. Med. Biol.* **2015**, *881*, 79.
[31] R. Ishizaka, Y. Hayashi, K. Iohara, M. Sugiyama, M. Murakami, T. Yamamoto, O. Fukuta, M. Nakashima, *Biomaterials* **2013**, *34*, 1888.
[32] P. J. Belt, I. C. Dickinson, D. R. B. Theile, *J. Plast. Reconstr. Aesthetic Surg.* **2005**, *58*, 425.
[33] H. Kärcher, M. Feichtinger, *J.Cranio-Maxillofacial Surg.* **2014**, *42*, 2056.
[34] S. A. Dowthwaite, J. Theurer, M. Belzile, K. Fung, J. Franklin, A. Nichols, J. Yoo, *JAMA Otolaryngol. – Head Neck Surg.* **2013**, *139*, 285.
[35] Y. Liu, J. K. Y. Chan, S. H. Teoh, *J. Tissue Eng. Regener. Med.* **2015**, *9*, 85.
[36] H. Fan, X. Zeng, X. Wang, R. Zhu, G. Pei, *Biomaterials* **2014**, *35*, 7407.
[37] X. Lan, Z. Sun, C. Chu, J. Boltze, S. Li, *Front. Neurol.* **2019**, *10*, 824.
[38] C. Gandia, A. Arminan, J. M. Garcia-Verdugo, E. Lledo, A. Ruiz, M. D. Minana, J. Sanchez-Torrijos, R. Paya, V. Mirabet, F. Carbonell-Uberos, M. Llop, J. A. Montero, P. Sepulveda, *Stem Cells* **2008**, *26*, 638.
[39] G. Z. Jin, H. W. Kim, *Tissue Eng. Regener. Med.* **2017**, *14*, 393.
[40] W. L. Dissanayaka, K. M. Hargreaves, L. Jin, L. P. Samaranayake, C. Zhang, *Tissue Eng., Part A* **2015**, *21*, 550.
[41] S. Guo, I. Redenski, S. Landau, A. Szklanny, U. Merdler, S. Levenberg, *Adv. Healthcare Mater.* **2020**, *9*, 2000974.
[42] T. Takebe, K. Sekine, M. Enomura, H. Koike, M. Kimura, T. Ogaeri, R. R. Zhang, Y. Ueno, Y. W. Zheng, N. Koike, S. Aoyama, Y. Adachi, H. Taniguchi, *Nature* **2013**, *499*, 481.
[43] P. Simon-Assmann, G. Orend, E. Mammadova-Bach, C. Spenle, O. Lefebvre, *Int. J. Dev. Biol.* **2011**, *55*, 455.
[44] X. Wang, D. T. Phan, A. Sobrino, S. C. George, C. C. Hughes, A. P. Lee, *Lab Chip* **2016**, *16*, 282.
[45] J. J. Moon, J. E. Saik, R. A. Poche, J. E. Leslie-Barbick, S. H. Lee, A. A. Smith, M. E. Dickinson, J. L. West, *Biomaterials* **2010**, *31*, 3840.
[46] D. R. Senger, K. P. Claffey, J. E. Benes, C. A. Perruzzi, A. P. Sergiou, M. Detmar, *Proc. Natl. Acad. Sci. USA* **1997**, *94*, 13612.
[47] J. Koffler, K. Kaufman-Francis, S. Yulia, E. Dana, A. P. Daria, A. Landesberg, S. Levenberg, *Proc. Natl. Acad. Sci. USA* **2011**, *108*, 14789.
[48] B. Li, C. Ruan, Y. Ma, Z. Huang, Z. Huang, G. Zhou, J. Zhang, H. Wang, Z. Wu, G. Qiu, *Tissue Eng., Part A* **2018**, *24*, 1413.

[49] P. Yang, X. Huang, J. Shen, C. Wang, X. Dang, H. Mankin, Z. Duan, K. Wang, *BMC Musculoskeletal Disord.* **2013**, *14*,318.
[50] H. Terheyden, P. Warnke, A. Dunsche, S. Jepsen, W. Brenner, S. Palmie, C. Toth, D. R. Rueger, *Int. J. Oral Maxillofac. Surg.* **2001**, *30*, 469.
[51] M. Zhou, X. Peng, C. Mao, F. Xu, M. Hu, G. Y. Yu, *Biomaterials* **2010**, *31*, 4935.
[52] W. P. Adams, A. H. Lipschitz, M. Ansari, J. M. Kenkel, R. J. Rohrich, *Ann. Plast. Surg.* **2004**, *53*, 6.
[53] D. Van Steenberghe, A. Callens, L. Geers, R. Jacobs, *Clin. Oral Implants Res.* **2000**, *11*, 210.
[54] Z. Schwartz, T. Weesner, S. Van Dijk, D. L. Cochran, J. T. Mellonig, C. H. Lohmann, D. L. Carnes, M. Goldstein, D. D. Dean, B. D. Boyan, *J. Periodontol.* **2000**, *71*, 1258.
[55] G. E. Friedlaender, D. M. Strong, K. W. Sell, *J. Bone Jt. Surg.* **1976**, *58*, 854.
[56] D. Chen, J. Y. Wu, K. M. Kennedy, K. Yeager, J. C. Bernhard, J. J. Ng, B. K. Zimmerman, S. Robinson, K. M. Durney, C. Shaeffer, O. F. Vila, C. Takawira, J. M. Gimble, X. E. Guo, G. A. Ateshian, M. J. Lopez, S. B. Eisig, G. Vunjak-Novakovic, *Sci. Transl. Med.* **2020**, *12*, eabb6683.
[57] Y. Yan, H. Chen, H. Zhang, C. Guo, K. Yang, K. Chen, R. Cheng, N. Qian, N. Sandler, Y. S. Zhang, H. Shen, J. Qi, W. Cui, L. Deng, *Biomaterials* **2019**, *190–191*, 97.
[58] A. Sterodimas, J. De Faria, B. Nicaretta, I. Pitanguy, *J. Plast. Reconstr. Aesthetic Surg.* **2010**, *63*, 1886.
[59] P. A. Zuk, M. Zhu, H. Mizuno, J. Huang, J. W. Futrell, A. J. Katz, P. Benhaim, H. P. Lorenz, M. H. Hedrick, *Tissue Eng.* **2001**, *7*, 211.
[60] M. M. L. Deckers, R. L. van Bezooijen, G. van der Horst, J. Hoogendam, C. van der Bent, S. E. Papapoulos, C. W. G. M. Löwik, *Endocrinology* **2002**, *143*, 1545.
[61] A. P. Kusumbe, S. K. Ramasamy, R. H. Adams, *Nature* **2014**, *507*, 323.
[62] S. K. Ramasamy, A. P. Kusumbe, L. Wang, R. H. Adams, *Nature* **2014**, *507*, 376.
[63] L. Shor, S. Guceri, R. Chang, J. Gordon, Q. Kang, L. Hartsock, Y. An, W. Sun, *Biofabrication* **2009**, *1*, 015003.
[64] C. X. Lam, D. W. Hutmacher, J. T. Schantz, M. A. Woodruff, S. H. Teoh, *J. Biomed. Mater. Res., Part A* **2009**, *90*, 906.
[65] C. Wei, L. Cai, B. Sonawane, S. Wang, J. Dong, *Biofabrication* **2012**, *4*, 025009.
[66] K. Hu, B. R. Olsen, *J. Clin. Invest.* **2016**, *126*, 509.
[67] P. B. Saadeh, B. J. Mehrara, D. S. Steinbrech, M. E. Dudziak, J. A. Greenwald, J. S. Luchs, J. A. Spector, H. Ueno, G. K. Gittes, M. T. Longaker, *Am. J. Physiol.* **1999**, *277*, C628.
[68] N. Hansen-Algenstaedt, C. Joscheck, L. Wolfram, C. Schaefer, I. Müller, A. Böttcher, G. Deuretzbacher, L. Wiesner, M. Leunig, P. Algenstaedt, W. Rüther, *Acta Orthop.* **2006**, *77*, 429.
[69] D. H. R. Kempen, L. Lu, A. Heijink, T. E. Hefferan, L. B. Creemers, A. Maran, M. J. Yaszemski, W. J. A. Dhert, *Biomaterials* **2009**, *30*, 2816.
[70] P. Pelissier, F. Villars, S. Mathoulin-Pelissier, R. Bareille, M.-H. Lafage-Proust, J. Vilamitjana-Amedee, M.-P. Simone, R. Bareille, L.-P. M.-H. H, V.-A. Joëlle, *Plast. Reconstr. Surg.* **2003**, *111*, 1932.
[71] C. Ferguson, E. Alpern, T. Miclau, J. A. Helms, *Mech. Dev.* **1999**, *87*, 57.
[72] K. M. Dupont, K. Sharma, H. Y. Stevens, J. D. Boerckel, A. J. García, R. E. Guldberg, *Proc. Natl. Acad. Sci. USA* **2010**, *107*, 3305.
[73] N. Harada, Y. Watanabe, K. Sato, S. Abe, K. Yamanaka, Y. Sakai, T. Kaneko, T. Matsushita, *Biomaterials* **2014**, *35*, 7800.
[74] X. Yu, X. Tang, S. V. Gohil, C. T. Laurencin, *Adv. Healthcare Mater.* **2015**, *4*, 1268.
[75] X. Wang, G. Wang, S. Zingales, B. Zhao, *Tissue Eng., Part B* **2018**, *24*, 463.
[76] J. M. Grasman, M. J. Zayas, R. L. Page, G. D. Pins, *Acta Biomater.* **2015**, *25*, 2.
[77] T. H. Qazi, D. J. Mooney, M. Pumberger, S. Geissler, G. N. Duda, *Biomaterials* **2015**, *53*, 502.
[78] S. P. Nukavarapu, D. L. Dorcemus, *Biotechnol. Adv.* **2013**, *31*, 706.
[79] H. H. Lu, S. D. Subramony, M. K. Boushell, X. Zhang, *Ann. Biomed. Eng.* **2010**, *38*, 2142.
[80] J. P. Spalazzi, S. B. Doty, K. L. Moffat, W. N. Levine, H. H. Lu, *Tissue Eng.* **2006**, *12*, 3497.
[81] A. Lesman, J. Koffler, R. Atlas, Y. J. Blinder, Z. Kam, S. Levenberg, *Biomaterials* **2011**, *32*, 7856.
[82] B. S. Kim, S. S. Yang, J. Lee, *J. Biomed. Mater. Res., Part B* **2014**, *102*, 943.
[83] B. Chuenjitkuntaworn, W. Inrung, D. Damrongsri, K. Mekaapiruk, P. Supaphol, P. Pavasant, *J. Biomed. Mater. Res., Part A* **2010**, *94*, 241.
[84] W. L. Grayson, S. Bhumiratana, C. Cannizzaro, P. H. G. Chao, D. P. Lennon, A. I. Caplan, G. Vunjak-Novakovic, *Tissue Eng., Part A* **2008**, *14*, 1809.
[85] A. B. Longo, S. M. Sacco, W. E. Ward, *J. Visualized Exp.* **2017**, *129*, e5636.
[86] A. P. Kusumbe, S. K. Ramasamy, A. Starsichova, R. H. Adams, *Nat. Protoc.* **2015**, *10*, 1904.